JMEPEG (2015) 24:2826–2835
DOI: 10.1007/s11665-015-1557-3

1059-9495/$19.00

The Grain Structure and Phase Transformations of TWIP Steel During Friction Stir Processing

M.H. Razmpoosh, A. Zarei-Hanzaki, S. Heshmati-Manesh, S.M. Fatemi-Varzaneh, and A. Marandi

(Submitted October 15, 2014; in revised form March 19, 2015; published online May 21, 2015)

The microstructural evolution of severely deformed twinning-induced plasticity steel was studied under various processing conditions. The material was subjected to the friction stir processing in three rotational speeds of 800, 1600, and 2000 rpm and at a constant traveling speed of 50 mm/min. It was found that the initial coarse-grained structure of the alloy (~40 μm) had been significantly refined in the processed zone (~0.8 μm). This substantial grain refinement was attributed to the extensive occurrence of dynamic recrystallization (DRX) in the course of deformation. Moreover, the Ferriteoscope results indicated a considerable drop in the ferrite volume fraction after processing under all of the applied rotational speeds. This was justified considering the reverse ferrite-to-austenite transformation. The present study has also explored the room-temperature mechanical properties of the processed material using microhardness measurement and tensile tests. The hardness profile coincides with the progression of DRX where the grain-refinement effect overcomes the hardness loss that resulted from decreasing the ferrite volume fraction. The lower formability of the friction stir processed material compared with the as-received metal was also explained by considering the suppression of mechanical twinning in the ultrafine-grained structure.

Keywords dual-phase steel, friction stir processing, twinning-induced plasticity steel, ultrafine grain

1. Introduction

As a response to improve the car fuel efficiency and gas emission issues, the automobile manufactures exert major efforts toward reducing the weight of the car bodies. Among the wide variety of the recently developed advanced high-strength steels (AHSS), twinning-induced plasticity (TWIP) steels are the most promising candidate to substitute the conventional steels owing to their proper strength-ductility combination. Recently, a new dual-phase (ferrite-austenite) TWIP steel has been developed and reported in the literature (Ref 1-3). Benefiting from the Fe-Mn-Al alloying system, the newly developed TWIP steel combines lower density and improved corrosion resistance (Ref 3, 4). In contrast to conventional TWIP steels, which are characterized by a fully austenitic microstructure, the new dual-phase steel contains a combination of ferrite and austenite at room temperature. In fact, the presence of considerable Al content of 6-9 wt.% increases the specific strength, and also stabilizes the ferrite phase at room temperature. The volume fraction of ferrite can be estimated using the isothermal sections of Fe-Mn-Al ternary systems (Ref 4, 5). It is worth noting that the addition of Al to fully austenitic high Mn steels would stimulate the formation of $(Fe, Mn)_3AlC_x$ carbides. Moreover, the Al addition also increases the stacking fault energy (SFE) of the alloy, and this in turn significantly influences the deformation mechanisms. However, the thermomechanical history might also influence the phase fractions (Ref 6). For example, it has been shown that an annealing process in the temperature range of 1000-1150 °C resulted in a higher ferrite volume fraction (Ref 7). Accordingly, the thermal-mechanical processing strategy can strongly dictate the final combination of ferrite-austenite volume fraction in the microstructure.

Severe plastic deformation (SPD), as a thermomechanical processing strategy, has provided new opportunities to enhance mechanical properties of metals and alloys by permitting grain refinement to the ultrafine and nano levels. These prospects have been attracting more and more research interest to the controversial issues, for instance, suppression of the mechanical twinning in the terms of the grain refinement. To date, few studies have been devoted to the processing of TWIP steels through utilization of SPD techniques. Matoso et al. (Ref 8) processed a TWIP steel holding 24% Mn through high-pressure torsion (HPT) method (up to 10 turns); this method resulted in ~100 nm grains. This was associated with a substantial increase of strength (hardness values). Bagherpour et al. (Ref 9) have also studied the possibility of TWIP steel processing by equal channel angular pressing (ECAP). It was reported that a single pass of ECAP had led to segmented flow as a result of flow localization where a gradient in microstructure was also observed. Furthermore, the latter research group could also successfully process a TWIP steel through shear extrusion (SE) technique (Ref 10). It was demonstrated that the twin fraction might increase and the twin spacing might decrease by the cumulative strain introduced through deformation channeling. Moreover, the crystallite sizes were determined as 710 and 500 nm after one pass SSE with the maximal distortion angles of 30° and 45°, respectively.

As a one-step SPD route, friction stir processing (FSP) techniques have attracted considerable interest and can provide

M.H. Razmpoosh, A. Zarei-Hanzaki, and **A. Marandi**, The Complex Laboratory of Hot Deformation and Thermomechanical Processing of High Performance Engineering Materials, School of Metallurgy and Materials Engineering, College of Engineering, University of Tehran, Tehran, Iran; **S. Heshmati-Manesh**, School of Metallurgy and Materials Engineering, College of Engineering, University of Tehran, Tehran, Iran; and **S.M. Fatemi-Varzaneh**, Shahid Rajaee Teacher Training University, Tehran, Iran. Contact e-mail: zareih@ut.ac.ir.

a localized modification and control of microstructures at near-surface layers of the processed metallic components (Ref 11). FSP techniques of soft metals such as aluminum and magnesium alloys (Ref 12-18) have been widely investigated; however, quite a small number of systematic studies may be found in the literature dealing with the FSP of steels. Due to the achievement of high temperatures during the FSP, the "hard-to-deform materials" can be processed successfully. During the FSP or welding of materials with higher melting points, such as steels, the tool materials hardly stand up to the high stresses and temperatures. The developments of tungsten alloys and polycrystalline cubic boron nitride (PCBN) have created FSP tools capable for processing steels (Ref 19, 20).

Sato et al. (Ref 21) studied the recrystallization behavior of 304L stainless steel during friction stirring by means of orientation imaging microscopy. As was expected, under the co-presence of the severe imposed strain and heat of the process, the dynamic recrystallization (DRX) occurs in the microstructure. Nevertheless, the nonuniform deformation associated with the processing may yield unequal distribution of dislocation densities. To this end, Xue et al. (Ref 22) have successfully friction-stir processed (FSPed) the plain low carbon steel, and an ultrafine ferrite/martensite dual-phase structure was obtained. The ultrafine polygonal ferrite grains (~1 μm) were distributed around the martensite phase, which consisted of nanostructured laths with a width of 200 nm. In another report by Mehranfar et al. (Ref 23), FSP was successfully used to produce the nanostructured layer on the super-austenitic steel. This led to a structural modification through breaking down the coarse sigma precipitates into the nanosized ones.

Despite the number of studies carried out on severely plastic deformed plain carbon steels (Ref 24), interstitial free steel (Ref 25), stainless steels (Ref 26), and tool steels (Ref 27), there is very little information in the literature in the case of twinning-induced plasticity (TWIP) steels. Accordingly, the current study is a part of a research program to explore the applicability of the FSP on TWIP steels. The microstructural evolution was discussed, and the mechanical properties of the processed material were evaluated using microhardness measurement along with a miniaturized tension testing.

2. Materials and Experimental Procedures

The experimental dual-phase TWIP steel was received in the form of an as-cast (electroslag remelted) ingot. In order to obtain a homogenized equiaxed microstructure, the ingot was hot forged at 1150 °C. To remove any segregation of the alloying elements (in particular Mn), the forged material was further annealed at 1150 °C for 45 min. The chemical composition of the experimental steel was Fe-0.06C-29.20Mn-0.60Si-5.20Al (wt.%), which was determined using the wet-chemistry analysis and inductively coupled plasma (ICP) method. The annealed material was cut to 3-mm-thick slices by wire electrodischarge machine (EDM), and the workpieces were subjected to FSP at three different rotational speeds (ω) of 800, 1600, and 2000 rpm under the constant travel speed of 50 mm/min. The FSP was performed using a vertical milling machine equipped with a tungsten-carbide base pinless tool with 8-mm diameter and 2° tilt angle. The preliminary processing using three speeds of 25, 50, and 100 mm/min showed that the sound, processed workpieces with no danger of crack could be obtained at travel speed of 50 mm/min. An argon atmosphere was used as the shielding gas under a polycarbonate box around the rotating tool and the workpiece to minimize surface oxidation during the process. The surfaces of the workpieces were polished up to 400 grit before the processing. The workpieces were clamped during on a backing plate. The peak temperatures during the processing were measured using a fixed type K Thermocouple. In order to suppress any grain growth and preserve the microstructure, the processed areas were quenched using water spray immediately after the processing. The processed workpieces were sectioned, ground, and polished for microstructural characterization. Optical microscopy (OM) and scanning electron microscopy (SEM) were utilized to examine the microstructures of the cross

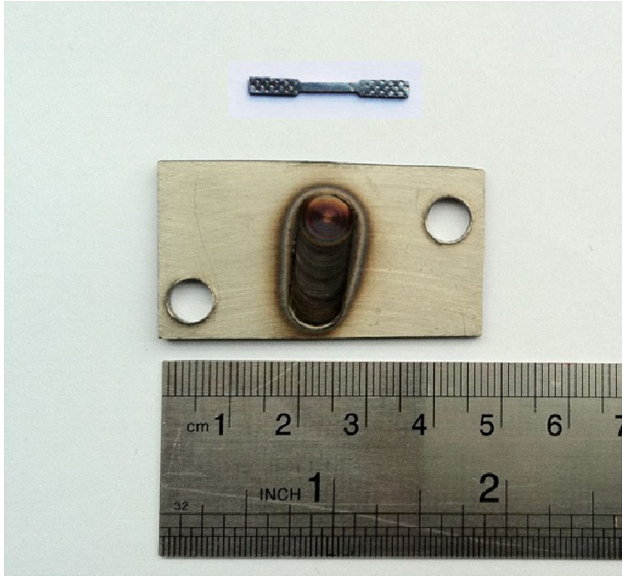

Fig. 1 The FSPed workpiece and tensile test specimens

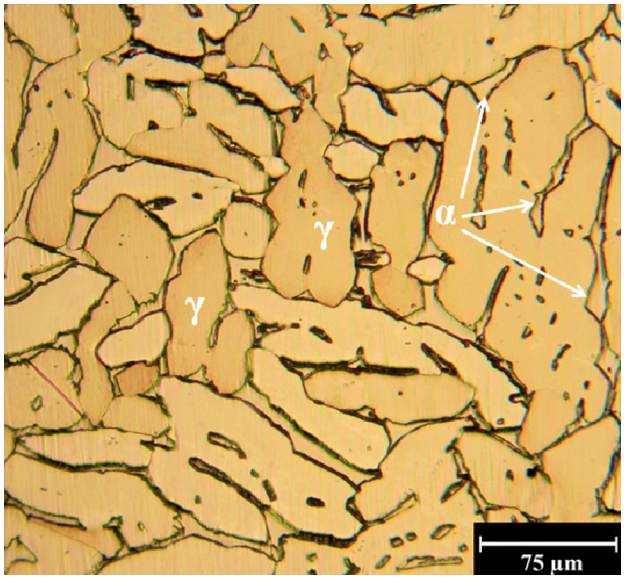

Fig. 2 The initial microstructure of the experimental dual-phase TWIP steel

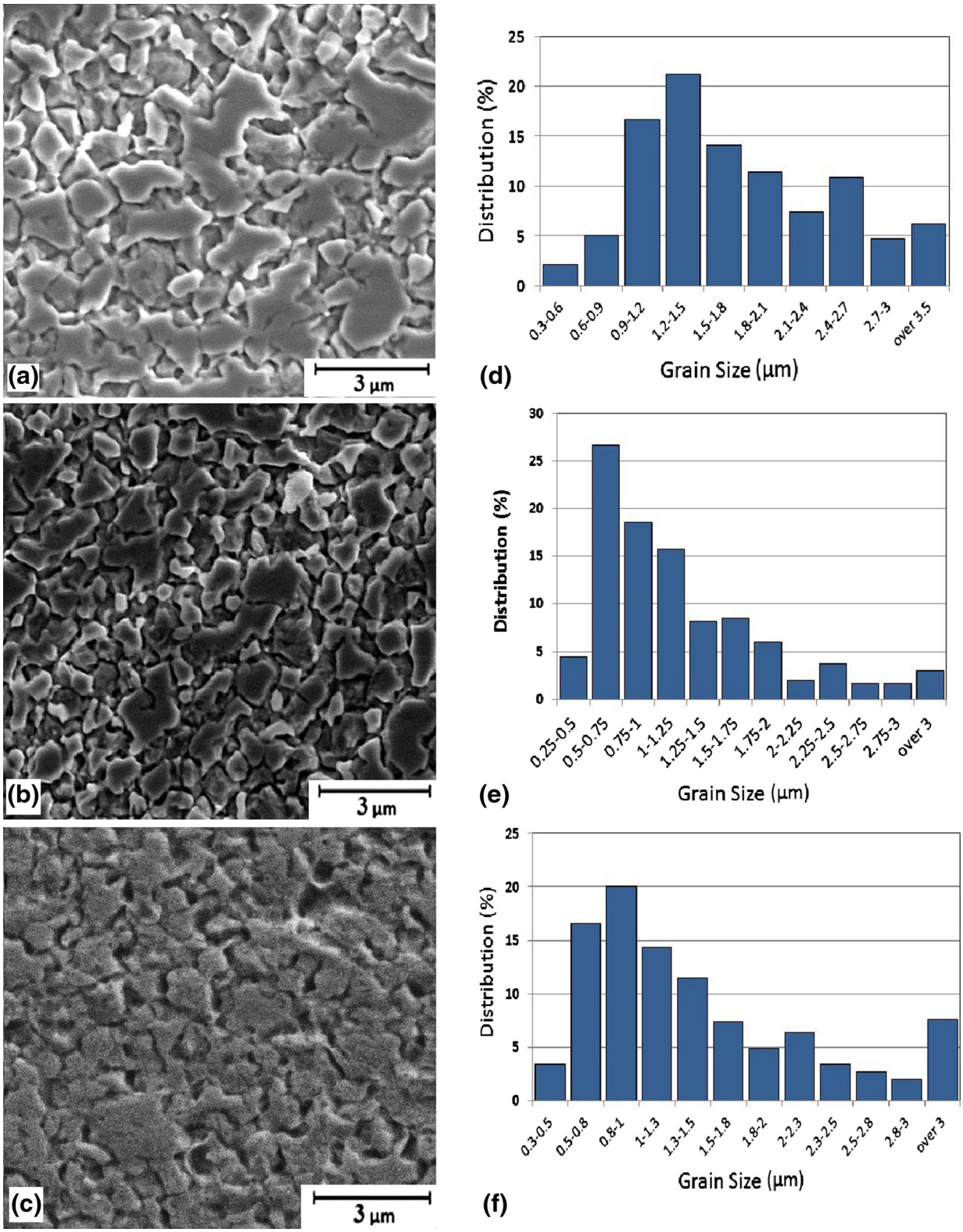

Fig. 3 The microstructure of the PZ at different rotational speeds and their corresponding grain size distribution: (a, d) ω = 800 rpm, (b, e) ω = 1600 rpm, (c, f) ω = 2000 rpm

section perpendicular to the processing direction (PD). The variation of ferrite volume fraction was measured by means of a Ferriteoscope FMP30 (Fischer), magneto-inductive device and CLEMEX image-analyzing software. X-ray diffraction (XRD) analyses were also done using a Philips-X'pert to identify the present microconstituents. Vickers microhardness measurements were made using a load of 200 g for 20 s. In order to evaluate the tensile properties, the sub-size plate-type tensile specimens (according to ASTM E8 (Ref 28)) with a gauge length of 7.2 mm and a width of 1.8 mm (Fig. 1) were cut by

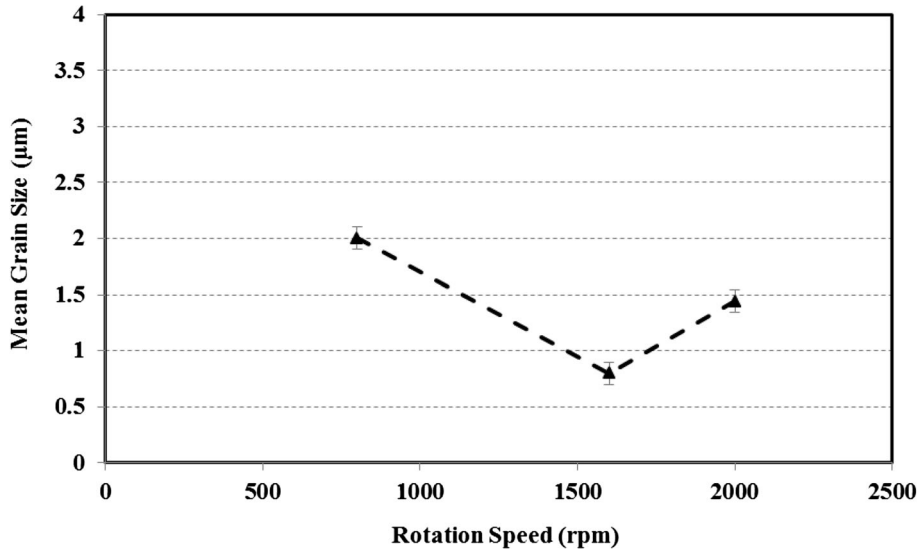

Fig. 4 The variation of mean grain size within the PZ with rotational speed

EDM in transverse direction; this was done in such a way that the gauge length could be located within the processed zone (PZ) (see Fig. 1), and be polished properly to attain smooth surfaces. Uniaxial tensile tests were conducted at room temperature using a universal testing machine (SANTAM STM50) under strain rate of 10^{-3} s^{-1}. The universal machine was equipped with a standard calibrated load cell holding the accuracy of 100 grf. The exact value of the specimen deformation was obtained through crosshead-displacement measurements by an encoder possessing the accuracy of ~0.03 mm. In order to assess the elongation-to-fracture values, the tensile specimens were gauge marked before any test, and the engineering fracture strain was obtained evaluating the final gauge length.

3. Results and Discussion

3.1 Microstructural Characterization

Figure 2 presents the initial microstructure of the base material (BM) in the annealed condition. The initial microstructure consists of a combination of ferrite and austenite with the volume fraction of about 30 and 70%, respectively. According to the ASTM E112 standard, the mean grain sizes were measured as 20 ± 3 μm for the ferrite and 40 ± 2 μm for the austenite phase. It is worth noting that the ferrite volume fraction was measured through OM image analyzer and confirmed by Ferriteoscopy.

The FSP on the experimental TWIP steel was successfully performed without cracking. To the best of the authors' knowledge, this has been never reported in the literature previously. The microstructures developed in the stir zone—hereafter called PZ—at different rotational speeds are shown in Fig. 3. The FSP has led to the formation of uniform fine-grained structure within the PZ at all three rotational speeds. This is related to the occurrence of DRX during the FSP. The mechanism by which the fine grains formed during the FSP is not yet understood (Ref 14). However, it is believed that the continuous dynamic recrystallization (CDRX) is mainly responsible for the formation of the ultrafine structure in the PZ (Ref 29). The grain size distribution of the PZ is also shown in Fig. 3. A mean grain size of 2 μm was measured for a rotational speed of 800 rpm (Fig. 3a), where most of the grain size frequency is in the range of 1-3 μm (Fig. 3d). As the rotational speed increases to 1600 rpm, the processing has resulted in the formation of grains with the mean size of 0.8 μm (Fig. 3b), which may be considered as the so-called ultrafine structure (Ref 30). In this case, the maximal frequency of the grains lies between 0.5 and 1 μm (Fig. 3e). However, further increase in the rotational speed to 2000 rpm resulted in a coarser mean grain size of 1.4 μm in the PZ (Fig. 3c). In this case, the grain sizes show a high frequency in the range of 0.8-2 μm (Fig. 3e). It is worth mentioning that the capability of the FSP in grain refining of austenite is comparable with the results reported for HPT (Ref 31, 32).

The effect of rotational speed on the PZ mean grain size is displayed in Fig. 4. Previous research also pointed out that there is an optimal rotational speed during the FSP of steels that yields the minimal grain size in the PZ (Ref 33). However, in the case of Al alloy, it has been reported that the grain sizes monotonically increase with the increasing rotational speed in a wide experimental range (Ref 29).

Heat is inevitably generated during the FSP by a combination of friction and energy dissipation through deformation of the material. Assuming a thermomechanical treatment imposed in the PZ, an increase in rotational speed increases the strain rate as well as temperature invoked during processing. In this regard, the Zener-Holloman parameter, which is defined as $Z = \dot{\varepsilon} \exp\left(\frac{Q}{RT}\right)$, dictates the size of the recrystallized grains through an inverse power law relationship (Ref 34). A higher rotational speed leads to a reduction in grain size via increased strain rate. This may also promote the grain growth by raising the processing temperature. It has been reported for Al alloys that the grain growth is the dominant factor in determining the recrystallized grain size (Ref 29). According to the present results, it appears that the strain rate is the controlling parameter where the rotational speed increases from 800 to 1600 rpm, thereby leading to finer grains. By contrast, where the rotational speed exceeds 1600 rpm, the dominant factor is the

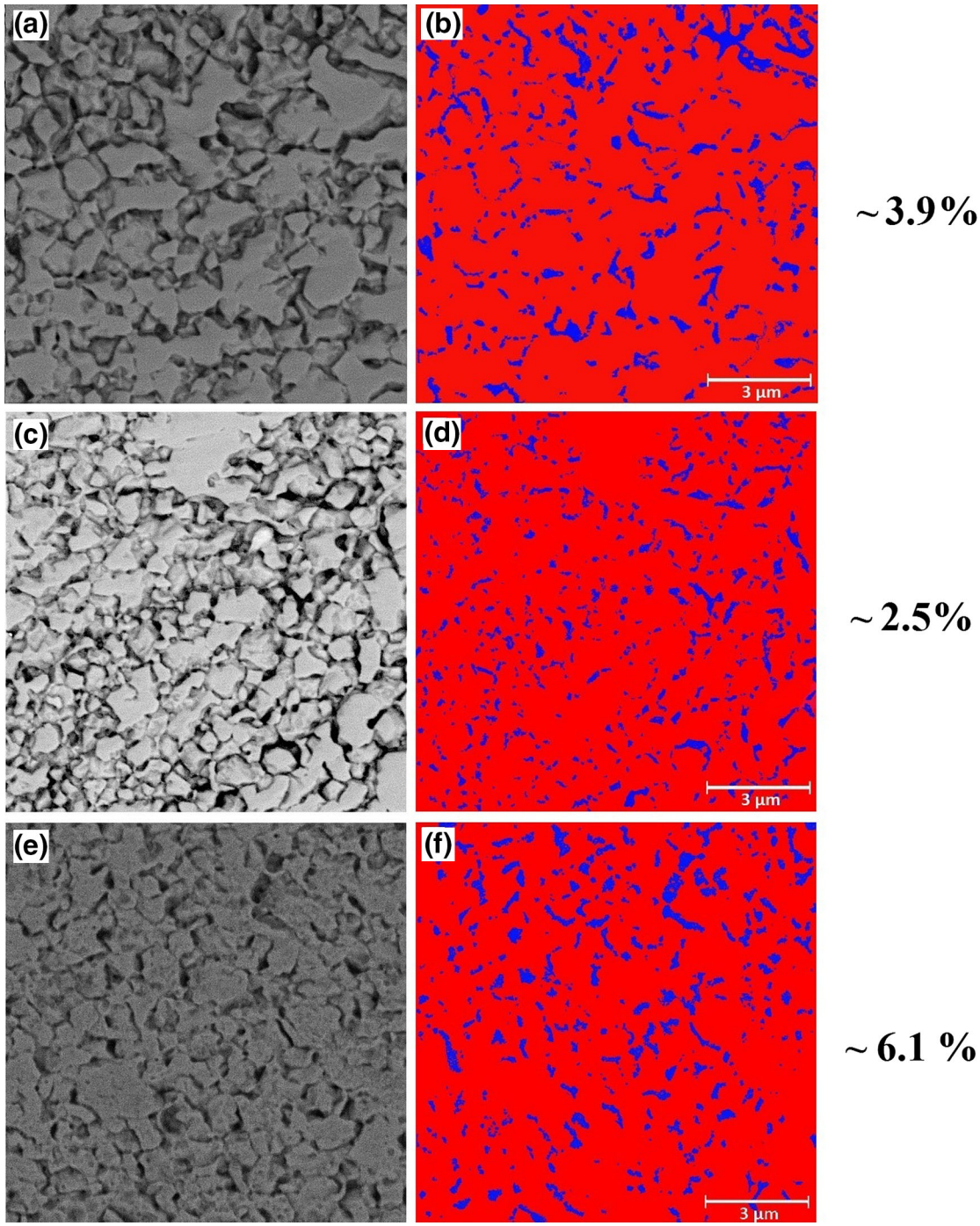

Fig. 5 The evolution of ferrite fraction within the PZ under different processing conditions utilizing BSE image analysis and corresponding Ferriteoscopy measurements, (a, b) ω = 800 rpm, (c, d) ω = 1600 rpm, and (e, f) ω = 2000 rpm

temperature; therefore the grain growth is promoted. The experimentally measured temperatures are in agreement with the aforementioned speculation, where temperatures of 863, 946, and 991 °C were recorded for 800, 1600, and 2000 rpm, respectively. Similar observation was previously made during the FSP of IF steel (Ref 33). This difference in the trends between Al alloys and the experimental TWIP steel is related, at least partly, to the differences in their specific heat capacity and thermal conductivity.

The evolution of ferrite fraction (FF) within the PZ under different processing conditions was examined through image analysis (Fig. 5). The obtained results were also supported through the Ferriteoscopy measurements. The XRD examination has also confirmed a substantial decrease in the FF after applying the FSP (Fig. 6). These results indicate very low FF after the processing under all conditions, while the initial material was composed of 30% ferrite. Furthermore, the trends of FF follow the grain size behavior by rotational speed; i.e., the FF is decreased by increasing the rotational speed from 800 to 1600 rpm, but increasing the speed to 2000 rpm has resulted in a higher FF. This can be attributed to the higher heat generation (i.e., higher temperatures reached) at higher rotational speeds (Fig. 7).

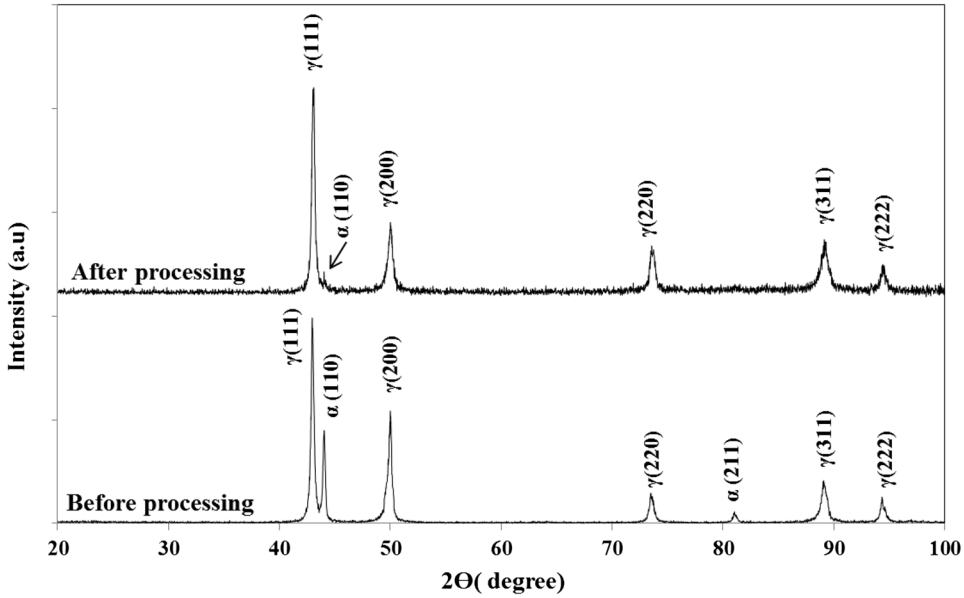

Fig. 6 The XRD patterns of the experimental steel before and after FSP at rotational speed of 1600 rpm

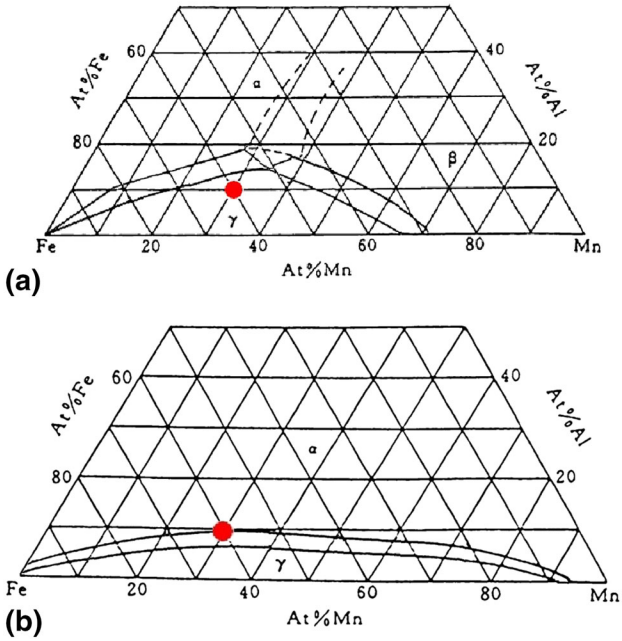

Fig. 7 The isothermal sections of the Fe-Mn-Al ternary system at (a) 900 °C and (b) 1200 °C (Ref 7) (the position of the experimental steel is shown by the red circle) (Color figure online)

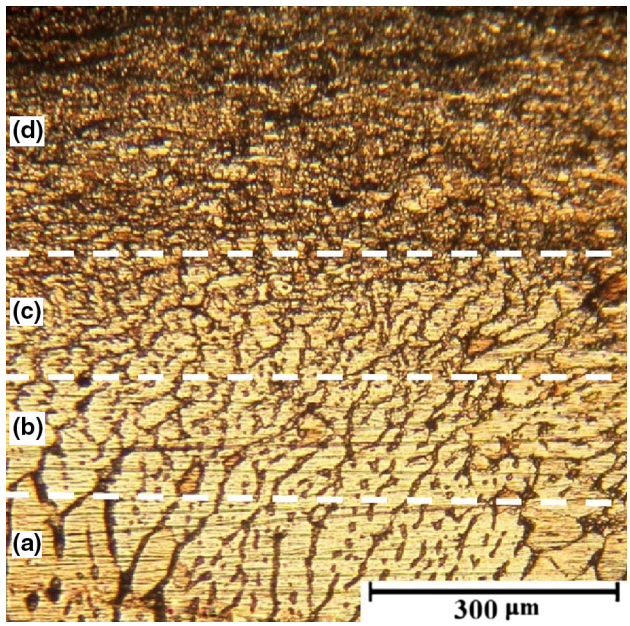

Fig. 8 The distinctly labeled microstructural zones of FSPed workpiece under rotational speed of 1600 rpm: (a) BM, (b) HAZ, (c) TMAZ, (d) PZ

The isothermal sections of Fe-Mn-Al equilibrium phase diagram at different temperatures are shown in Fig. 8 (Ref 7). As indicated, the composition of the experimental steel (Fe-30Mn-5Al) at lower temperatures ($T < 1000$ °C) is located in the austenite single-phase region. Thus, the as-annealed material (initial workpiece) which contains austenite and ferrite is potentially metastable. By increasing the temperature during the FSP, the transformation of ferrite to austenite (equilibrium phase) is stimulated. Thus, a significant drop in the FF may be rationalized. The higher the rotational speed employed, the higher the temperature created during the FSP. The latter, in turn, increases the kinetics of the ferrite-to-austenite transformation; however, since the temperature reaches the highest by applying 2000 rpm as the rotational speed, the material may be positioned in the austenite + ferrite two-phase region (Fig. 6).

The microstructure of the sample cut from the section perpendicular to the PD is illustrated in Fig. 8. Different microstructural zones were identified; zone (a) is base metal with a dual-phase coarse-grained microstructure; the next two transitional zones, labeled as (b) and (c), are the heat-affected zone (HAZ) and the thermomechanically affected zone

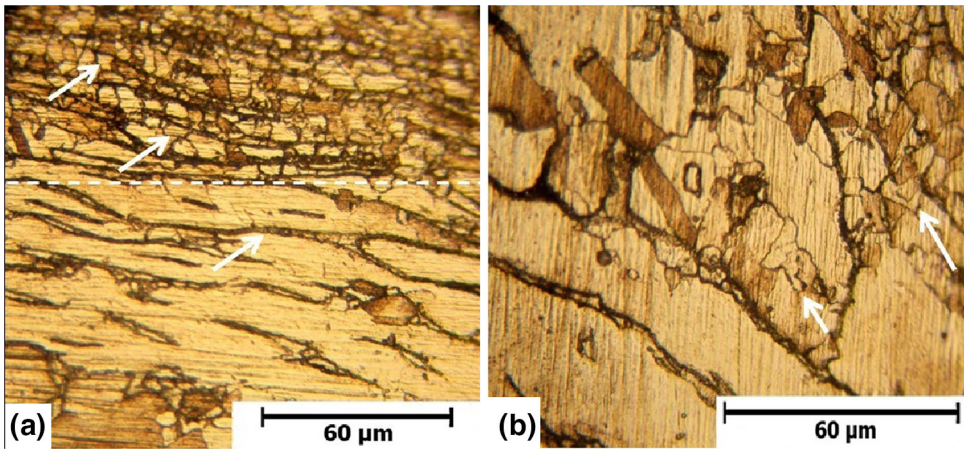

Fig. 9 The microstructure of the FSPed workpiece under rotational speed of 1600 rpm; (a) the upper and lower TMAZ, (b) the occurrence of DRX in austenite grains

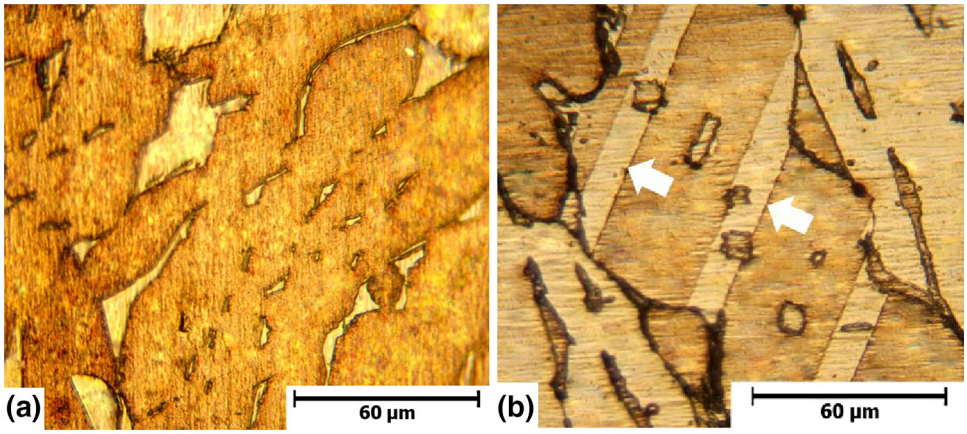

Fig. 10 (a) The austenite grain structure within the HAZ, (b) the annealing twins within the HAZ

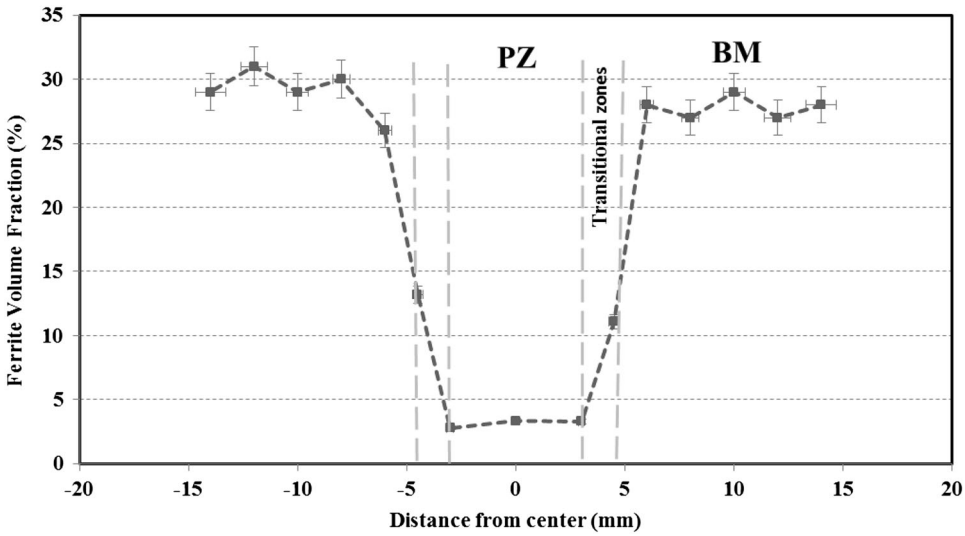

Fig. 11 The variation of the ferrite volume fraction within the PZ under a rotational speed of 1600 rpm

(TMAZ); respectively. Zone (d) is the PZ, which has been discussed earlier.

The TMAZ (region B in Fig. 8), which is a distinct region next to the PZ, would experience both heat and deformation. However, in the present condition, the heat and deformation were insufficient to cause significant progression in recrystallization. In this region, initial grains are generally elongated along the material flow lines. For the sake of better characterization, a detailed microscopic examination of the TMAZ was performed. Figure 9 shows that a gradient in the microstructure has been developed in this region, where upper and lower sub-regions were identified. This is related to the strain and temperature gradients spread over the TMAZ. As such, a partial recrystallization of the austenite grains has taken place at the upper areas, whereas the lower regions include the deformed grains with no recrystallization.

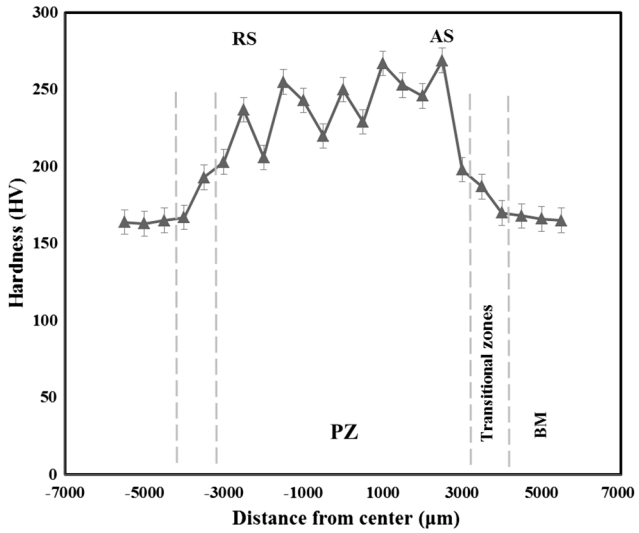

Fig. 12 The microhardness profile of the FSPed material under a rotational speed of 1600 rpm; AS is for advancing side and RS for retreating side

The grain size measurement implies a significant grain growth in the HAZ (Fig. 10a). Moreover, the frequent formation of annealing twins is observed in the HAZ (Fig. 10b). The formation of annealing twins during thermal treatment is known as a characteristic microstructural feature of FCC alloys holding low SFE. The appearance of twins is discussed considering the grain boundary dissociation model, where the shape of twin is determined by the need to minimize interfacial energy (Ref 35).

The variation of the FF along the investigated zones has been examined using Ferriteoscopy. As seen in Fig. 11, a gradient in the FF is found in the transitional zones formed after the FSP at 1600 rpm. This may be discussed relying on the ferrite-to-austenite transformation scheme. Considering the diffusional nature of ferrite-to-austenite transformation, the higher the temperature a zone reached the more the transformation progressed. Thus, the observed FF gradient results from the temperature gradient introduced during the FSP.

3.2 Mechanical Characterization

Microhardness measurements were used to trace the homogeneity of mechanical properties across the aforementioned

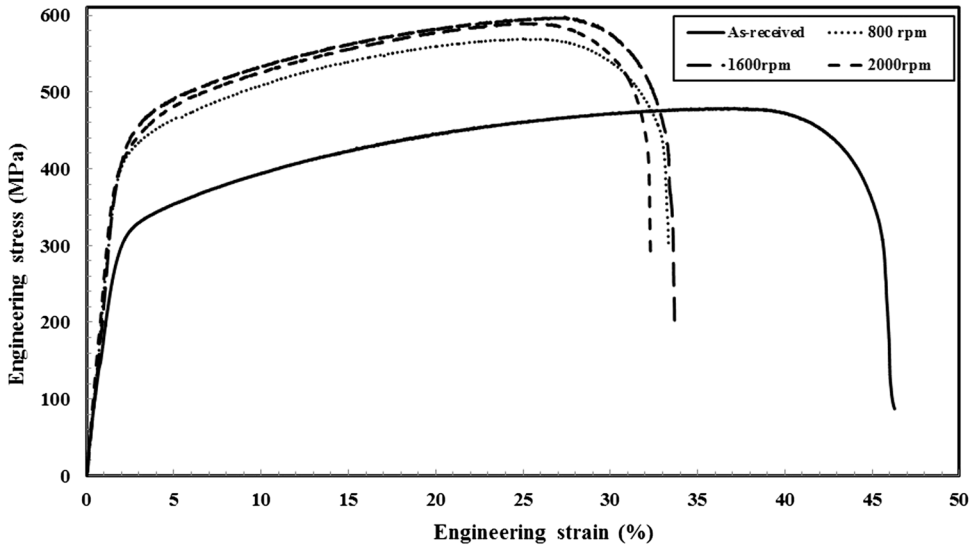

Fig. 13 Tensile engineering stress-strain curves of the as-received and processed (under ω = 800, 1600, and 2000 rpm) specimens

Table 1 The tensile properties of the as-received and processed materials

Specimen	Mean grain size, μm	Ferrite volume fraction, %	YS, MPa	UTS, MPa	TEL, %
As-received	40	30	304	478	46.4
800 rpm	2	3.9	412	569	33.2
1600 rpm	0.8	2.5	431	597	33.8
2000 rpm	1.4	6.1	420	589	32.1

zones. Figure 12 illustrates the microhardness profile for the processed workpiece under the rotational speed of 1600 rpm as a function of the distance from the process centerline. The higher microhardness values indicate the progression of DRX (considering Hall-Petch effect) from the lower TMAZ toward the PZ, where the upper and lower TMAZs have experienced lower degree of recrystallization (Fig. 8). It should be noted that the ferrite phase is characterized by a higher hardness in the experimental steel (Ref 2), so the results implied that the grain refinement may overcome the hardness loss resulting from the decrease in the FF.

The mechanical properties of the initial and processed materials under 800, 1600, and 2000 rpm were examined by tensile testing method (Fig. 13). The tensile properties of the initial and processed materials are tabulated in Table 1. The results demonstrate an improved yield strength (YS) and ultimate tensile strength (UTS) in the processed materials for all the applied rotational speeds. As is seen, the maximal YS and UTS are obtained under rotational speed of 1600 rpm. The rotational speeds of 2000 and 800 rpm, however, result in lower YS and UTS in the processed materiel. This is connected to the larger grain sizes obtained after processing steps under rotational speeds of 2000 and 800 rpm. As is observed, the total elongation (TEL) is reduced after processing. The ductility deterioration is rationalized considering the suppression of mechanical twins in the ultrafine-grained FSPed material. Accordingly, twinning hardly contributes to plasticity during tensile deformation, and the work hardenability of the materials rapidly becomes exhausted. The elongation-to-fracture of the processed materials is decreased by increasing the FF. Accordingly, the processed material under the rotational speed of 1600 rpm possesses the highest TEL since it consists of the lowest FF. This is completely consistent with the results reported by Imandoust et al. (Ref 4).

4. Conclusions

A dual-phase twinning-induced plasticity steel (TWIP) was successfully FSPed using a tungsten-carbide base tool under different rotational speeds. An optimal rotational speed of 1600 rpm was determined to achieve the ultrafine-grained microstructure. The obtained substantial grain refinement was attributed to the enhanced operation of DRX in the course of deformation. DRX was also characterized at the upper TMAZ, while the HAZ exhibited no recrystallization. The ferrite-to-austenite transformation took place during processing, the progression of which coincided with the zone temperature increment. This resulted in decreased ferrite volume fraction after the processing. The microhardness measurement showed higher values at the PZ and the upper TMAZ due to the finer mean grain sizes. The grain refinement overcame the hardness loss resulting from the decrease in the FF. It was also found that the fine-grained structure of the FSPed material suppresses the contribution of twins during tensile deformation which would degrade the ductility values.

References

1. V. Torabinejad, A. Zarei-Hanzaki, S. Moemeni, and A. Imandoust, An Investigation to the Microstructural Evolution of Fe-29Mn-5Al Dual-Phase Twinning-Induced Plasticity Steel Through Annealing, *Mater. Des.*, 2011, **32**(10), p 5015–5021
2. V. Torabinejad, A. Zarei-Hanzaki, M. Sabet, and H.R. Abedi, The Effect of Low Temperature Annealing on the Mechanical Behavior of Cold Rolled Dual-Phase Twinning-Induced Plasticity Steel, *Mater. Des.*, 2011, **32**(4), p 2345–2349
3. A. Imandoust, A. Zarei-Hanzaki, and H.R. Abedi, Low-Temperature Strain-Induced Ferrite Transformation in Twinning-Induced Plasticity Steel, *Scr. Mater.*, 2012, **67**(12), p 995–998
4. A. Imandoust, A. Zarei-Hanzaki, S. Heshmati-Manesh, S. Moemeni, and P. Changizian, Effects of Ferrite Volume Fraction on the Tensile Deformation Characteristics of Dual Phase Twinning Induced Plasticity Steel, *Mater. Des.*, 2014, **53**, p 99–105
5. A. Imandoust, A. Zarei-Hanzaki, M. Sabet, and H.R. Abedi, An Analysis of the Deformation Characteristics of a Dual Phase Twinning-Induced Plasticity Steel in Warm Working Temperature Regime, *Mater. Des.*, 2012, **40**, p 556–561
6. A. Mohamadizadeh, A. Zarei-Hanzaki, S. Heshmati-Manesh, and A. Imandoust, The Effect of Strain Induced Ferrite Transformation on the Microstructural Evolutions and Mechanical Properties of a TRIP-Assisted Steel, *Mater. Sci. Eng. A*, 2014, **607**, p 621–629
7. W.C. Cheng, H.Y. Lin, and C.F. Liu, Observing the Massive Transformation in an Fe-Mn-Al Alloy, *Mater. Sci. Eng. A*, 2002, **335**(1), p 82–88
8. M.S. Matoso, R.B. Figueiredo, M. Kawasaki, D.B. Santos, and T.G. Langdon, Processing a Twinning-Induced Plasticity Steel by High-Pressure Torsion, *Scr. Mater.*, 2012, **67**(7–8), p 649–652
9. E. Bagherpour, M. Reihanian, and R. Ebrahimi, On the Capability of Severe Plastic Deformation of Twining Induced Plasticity (TWIP) Steel, *Mater. Des.*, 2012, **36**, p 391–395
10. E. Bagherpour, M. Reihanian, and R. Ebrahimi, Processing Twining Induced Plasticity Steel Through Simple Shear Extrusion, *Mater. Des.*, 2012, **40**, p 262–267
11. F. Nascimento, T. Santos, P. Vilaça, R.M. Miranda, and L. Quintino, Microstructural Modification and Ductility Enhancement of Surfaces Modified by FSP in Aluminium Alloys, *Mater. Sci. Eng. A*, 2009, **506**(1–2), p 16–22
12. Z.Y. Ma, S.R. Sharma, and R.S. Mishra, Effect of Multiple-Pass Friction Stir Processing on Microstructure and Tensile Properties of a Cast Aluminum-Silicon Alloy, *Scr. Mater.*, 2006, **54**(9), p 1623–1626
13. C.I. Chang, X.H. Du, and J.C. Huang, Achieving Ultrafine Grain Size in Mg-Al-Zn Alloy by Friction Stir Processing, *Scr. Mater.*, 2007, **57**(3), p 209–212
14. J.Q. Su, T.W. Nelson, and C.J. Sterling, Friction Stir Processing of Large-Area Bulk UFG Aluminum Alloys, *Scr. Mater.*, 2005, **52**(2), p 135–140
15. B. Mansoor and A.K. Ghosh, Microstructure and Tensile Behavior of a Friction Stir Processed Magnesium Alloy, *Acta Mater.*, 2012, **60**(13–14), p 5079–5088
16. C.I. Chang, X.H. Du, and J.C. Huang, Producing Nanograined Microstructure in Mg-Al-Zn Alloy by Two-Step Friction Stir Processing, *Scr. Mater.*, 2008, **59**(3), p 356–359
17. Y.N. Wang, C.I. Chang, C.J. Lee, H.K. Lin, and J.C. Huang, Texture and Weak Grain Size Dependence in Friction Stir Processed Mg-Al-Zn Alloy, *Scr. Mater.*, 2006, **55**(7), p 637–640
18. W. Woo, H. Choo, D.W. Brown, P.K. Liaw, and Z. Feng, Texture Variation and Its Influence on the Tensile Behavior of a Friction-Stir Processed Magnesium Alloy, *Scr. Mater.*, 2006, **54**(11), p 1859–1864
19. J.D. Escobar, E. Velásquez, T.F.A. Santos, A.J. Ramirez, and D. López, Improvement of Cavitation Erosion Resistance of a Duplex Stainless Steel Through Friction Stir Processing (FSP), *Wear*, 2013, **297**(1–2), p 998–1005
20. S. Dodds, A.H. Jones, and S. Cater, Tribological Enhancement of AISI, 420 Martensitic Stainless Steel Through Friction-Stir Processing, *Wear*, 2013, **302**(1–2), p 863–877
21. Y.S. Sato, T.W. Nelson, and C.J. Sterling, Recrystallization in Type 304L Stainless Steel During Friction Stirring, *Acta Mater.*, 2005, **53**(3), p 637–645
22. P. Xue, B.L. Xiao, W.G. Wang, Q. Zhang, D. Wang, Q.Z. Wang, and Z.Y. Ma, Achieving Ultrafine Dual-Phase Structure with Superior Mechanical Property in Friction Stir Processed Plain Low Carbon Steel, *Mater. Sci. Eng. A*, 2013, **575**, p 30–34
23. M. Mehranfar and K. Dehghani, Producing Nanostructured Super-Austenitic Steels by Friction Stir Processing, *Mater. Sci. Eng. A*, 2011, **528**(9), p 3404–3408

24. F. Khodabakhshi and M. Kazeminezhad, The Effect of Constrained Groove Pressing on Grain Size, Dislocation Density and Electrical Resistivity of Low Carbon Steel, *Mater. Des.*, 2011, **32**(6), p 3280–3286
25. O. Saray, G. Purcek, I. Karaman, T. Neindorf, and H.J. Maier, Equal-Channel Angular Sheet Extrusion of Interstitial-Free (IF) Steel: Microstructural Evolution and Mechanical Properties, *Mater. Sci. Eng. A*, 2011, **528**(21), p 6573–6583
26. S. Qu, C.X. Huang, Y.L. Gao, G. Yang, S.D. Wu, Q.S. Zang, and Z.F. Zhang, Tensile and Compressive Properties of AISI, 304L Stainless Steel Subjected to Equal Channel Angular Pressing, *Mater. Sci. Eng. A*, 2008, **475**(1–2), p 207–216
27. Y. Morisada, H. Fujii, T. Mizuno, G. Abe, T. Nagaoka, and M. Fukusumi, Nanostructured Tool Steel Fabricated by Combination of Laser Melting and Friction Stir Processing, *Mater. Sci. Eng. A*, 2009, **505**(1–2), p 157–162
28. ASTM, *Standard Test Methods for Tension Testing of Metallic Materials*, ASTM E8, Annual Book of ASTM Standards, West Conshohocken, 2010
29. R.S. Mishra and Z.Y. Ma, Friction Stir Welding and Processing, *Mater. Sci. Eng. R*, 2005, **50**(1–2), p 1–78
30. Y. Weng, *Ultra-Fine Grained Steels*, Springer, Berlin, 2009
31. A. Vorhauer, S. Kleber, and R. Pippan, Influence of Processing Temperature on Microstructural and Mechanical Properties of High-Alloyed Single-Phase Steels Subjected to Severe Plastic Deformation, *Mater. Sci. Eng. A*, 2005, **410–411**, p 281–284
32. Y. Mine, K. Tachibana, and Z. Horita, Grain-Boundary Diffusion and Precipitate Trapping of Hydrogen in Ultrafine-Grained Austenitic Stainless Steels Processed by High-Pressure Torsion, *Mater. Sci. Eng. A*, 2011, **528**(28), p 8100–8105
33. K. Dehghani and A. Chabok, Dependence of Zener Parameter on the Nanograins Formed During Friction Stir Processing of Interstitial Free Steels, *Mater. Sci. Eng. A*, 2011, **528**(13–14), p 4325–4330
34. C.I. Chang, C.J. Lee, and J.C. Huang, Relationship Between Grain Size and Zener-Holloman Parameter During Friction Stir Processing in AZ31Mg Alloys, *Scr. Mater.*, 2004, **51**(6), p 509–514
35. Y. Jin, B. Lin, M. Bernacki, G.S. Rohrer, A.D. Rollett, and N. Bozzolo, Annealing Twin Development During Recrystallization and Grain Growth in Pure Nickel, *Mater. Sci. Eng. A*, 2014, **597**, p 295–303